

RAPID COMMUNICATION

Spatially heterogeneous carbon-fiber papers as surface dendrite-free current collectors for lithium deposition

Xiulei Ji, De-Yu Liu, Daniel G. Prendiville, Yichi Zhang, Xiaonao Liu, Galen D. Stucky*

Department of Chemistry and Biochemistry, University of California, Santa Barbara, CA 93106-9510, United States

Received 25 August 2011; received in revised form 7 November 2011; accepted 28 November 2011
Available online 9 January 2012

KEYWORDS

Lithium dendrite;
Current collector;
Line-of-sight
deposition;
Spatial
heterogeneity;
Insulating

Summary Despite the high energy density, the lithium metal electrode has been plagued for decades with a dendrite growth problem that can result in a battery thermal runaway. Here, we introduce anisotropic spatially heterogeneous three dimensional (3D) current collectors that prevent lithium deposition on the insulating electrolyte-facing surface and accommodate lithium deposition inside the spacious voids. The anisotropic spatial heterogeneity was introduced by a line-of-sight deposition of a thin SiO₂ layer onto a carbon-fiber paper. The deposited SiO₂ was later converted into SiC by a magnesiothermic reaction. The SiO₂ and SiC decorated 3D current collectors were confirmed dendrite-free by ex situ SEM observation after a deep lithium deposition of 28.8 C cm⁻² at a high current density of 4 mA cm⁻². A high lithium cycling efficiency of 94% was achieved over deep deposition (14.4 C cm⁻²) and stripping cycles in a carbonate based organic electrolyte, demonstrating the superiority of the novel current collector for dendrite control and lithium cycling. This strategy opens new avenues to address the dendrite problem by rationally designed current collectors and for the creation of a high energy density electrode.

© 2011 Elsevier Ltd. All rights reserved.

Introduction

A metallic lithium electrode is energetically attractive in that it can theoretically provide a gravimetric capacity of 3861 mA h g⁻¹, more than 10 times that of lithiated carbona-

ceous anodes [1] (339 mA h g⁻¹ for LiC₆) at a very low redox potential (-3.04 V vs. Standard Hydrogen Electrode). The earliest rechargeable lithium batteries (LBs) in the 1970s and 1980s used lithium metal as the negative electrode in prototypes [2] and were introduced as commercial products [3]. However, it was quickly recognized that despite the high energy density, metallic lithium electrodes are unsafe and unreliable due to the lithium dendrite growth during electrodeposition [4–6]. The dendrites are associated with nearly all the failure mechanisms of the

* Corresponding author. Tel.: +1 805 893 4872;
fax: +1 805 893 4120.

E-mail address: stucky@chem.ucsb.edu (G.D. Stucky).

LBs and can lead to a battery thermal runaway [7–9]. The so called “rocking-chair principle” was introduced three decades ago to address the dendrite problem [10,11]. The improved battery safety is at a significant cost of energy density with lithium ions reversibly commuting between bulky intercalation electrodes. The rocking-chair principle has led to the tremendous success of lithium-ion batteries (LIBs), for portable and moderately powered electronic applications. After two decades of relentless optimization, the LIBs based on this topotactic chemistry have nearly reached the maximum energy density and power [12–14].

There is an increasing major need for more compact energy storage systems that exhibit the higher power metrics required to facilitate strategic applications, particularly for electrified transportation and load-leveling for intermittent renewable energy sources. The conventional LIB configurations with carbonaceous or carbon–metal composite [15] anodes with limited capacities will not meet the demand for high energy density batteries [16]. High energy Li–sulfur [17] and Li–air [18] LBs are considered as the most promising candidates to meet the demands. In these devices, improved cathode configurations have been reported [19–21]; however, the dendrite problem remains as a significant and unsolved restriction for the LBs [22].

Intensive efforts have been made to understand and address the dendrite growth problem. Chazalviel proposed a theoretical model which explained that, at high current densities, the dendrite growth is due to the large electric field induced by the anion depletion near the cathode [23]. The model also predicted that dendrite growth would not be observed at low current densities due to the non-zero anionic concentration. This was contradicted by the experimental observation by Rosso et al. who attributed the dendrites observed at low current densities from 0.02 to 0.3 mA cm⁻² to the inhomogeneities on the electrode surface [24]. They proposed another model that describes the uneven concentration distribution of the electrolyte as being caused by specific properties of the lithium/electrolyte system. Depleted zones of anions may appear as soon as the correlation length of the inhomogeneities is large enough.

Dry polymer [25] and gel polymer [26,27] electrolytes with better mechanical properties have been found effective in controlling the dendrite growth. Recently, ionic liquids have attracted some attention due to their better cathodic stability towards lithium metal than other liquid electrolytes [28,29]. Another approach is to control the physio-chemical properties of lithium metal/electrolyte interphase by protection layers. Reactions between lithium metal and electrolyte additives [30,31] or sol–gel precursors [32,33] were employed to form solid electrolyte interphase (SEI) protection layers. Polymer films [34,35] were also investigated as protective coatings. Impermeable multi-layer structures, composed of an outer Li-ion containing glass-ceramic layer [36–38], and an inner layer made of Li₃N (or LiF, or LiI) [39] or polymers [40] compatible with lithium metal, can give rise to water-stable lithium anodes [41]. The surface protection approaches greatly enhance the compatibility between lithium anodes and organic electrolytes. However, the intrinsic uneven lithium electrodeposition still

results in a stress buildup beneath the protection layers [42,43].

It must be emphasized that nearly all the previous efforts were made using flat lithium foil/film or 2D metal foil current collectors. Although designed electrode materials with function precisely controlled have shown great potential [44], rationally designed current collectors have rarely been taken into account in solving the dendrite problem. Inspired by the enhanced electrode performances by 3D current collectors [45–48], herein we report surface dendrite-free lithium deposition created by using spatially heterogeneous 3D current collectors. The task is to confine lithium metal deposition inside the 3D current collectors. A major hurdle in accomplishing this is the conductive electrolyte-facing surface of the 3D current collectors, which provides favorable sites for lithium deposition and dendrite growth while leaving the interior voids empty. Our solution to this challenge is to introduce an anisotropic spatial heterogeneity in terms of conductivity for the 3D current collectors by insulating the electrolyte-facing surface while keeping the other parts conductive. This will fundamentally prevent inter-electrode dendrite growth and force lithium deposition inside the large voids.

Materials and methods

Preparation of SiO₂-carbon-fiber paper (SiO₂-CP). CP (Model: 2050 A) was purchased from Fuel Cell Store, Inc. SiO₂ crystals (99.99%) was used as the SiO₂ source. The electron-beam deposition of SiO₂ onto CP was carried out at a rate of ~1 Å per second until a set thickness of 50 nm was reached by an instrument of Airco Temescal (Model CV-8).

Preparation of SiC-CP samples

SiO₂-CP was placed covering an alumina boat with the SiO₂ decorated side facing magnesium power located in the alumina boat. The reaction experimental setup is schematically shown in Fig. 1. Note that magnesiothermic reactions are normally carried out at 650–700 °C. In our study, to overcome the low reactivity of highly graphitic CP fibers, the reaction was conducted at 800 °C for 2 h with an excess of metallic magnesium source under an argon flow. The reacted carbon paper samples were soaked in 2 M HCl overnight in

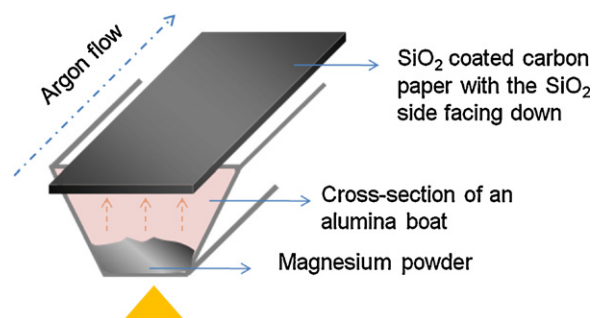


Figure 1 Schematic illustrating the experimental setup of the magnesiothermic reaction to convert SiO₂-CP to SiC-CP. The SiO₂ decorated side of the carbon paper directly faces hot magnesium vapor during the reaction.

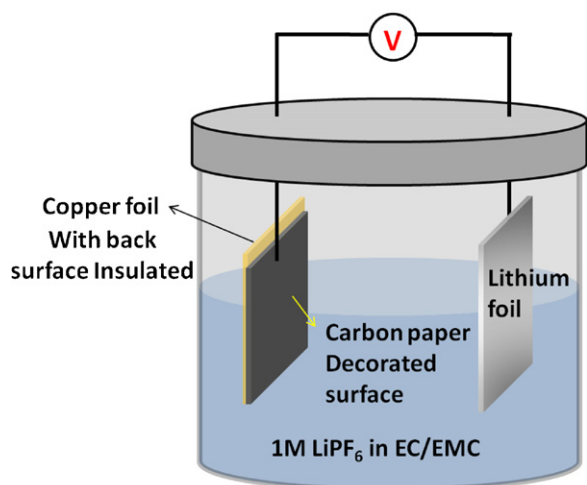


Figure 2 Schematic showing the vial cell setup for the electrochemical studies. Only one side of the (SiO₂-) CP electrode is allowed to expose to the electrolyte.

order to remove the formed MgO and possible Mg₂Si. Before lithium deposition, the SiC decorated paper samples were soaked in 50% (weight) HF aqueous solution overnight to remove as-formed silicon.

Physical characterizations

Powder X-ray diffraction (XRD) patterns were collected on a Scintag PADX diffractometer with Cu K α radiation (45 kV, 35 mA). Scanning electron microscopy (SEM) images were acquired on a FEI XL40 Sirion FEG digital scanning electron microscope. Prior to the SEM measurements, the vial cells were dismantled in an argon-filled glove box. The electrodes taken from the vial cells were rinsed by dry tetrahydrofuran (THF) to remove the residual electrolytes and later on dried under vacuum at room temperature. Nitrogen sorption isotherms were measured at -196°C on a Micromeritics Tristars 3000 analyzer. Before measurements, the samples were degassed on a vacuum line at 150°C overnight. In X-ray photon spectra (XPS) measurements, we use the peak of carbon 1s signal from a pure carbon sample to calibrate the spectrum.

Electrochemical characterizations

Electrochemical studies were carried out in vial cells on an EC-lab VMP3 instrument at room temperature. The transparent vial cells were deliberately used for the convenience of in situ visual inspection of the dendrite growth during

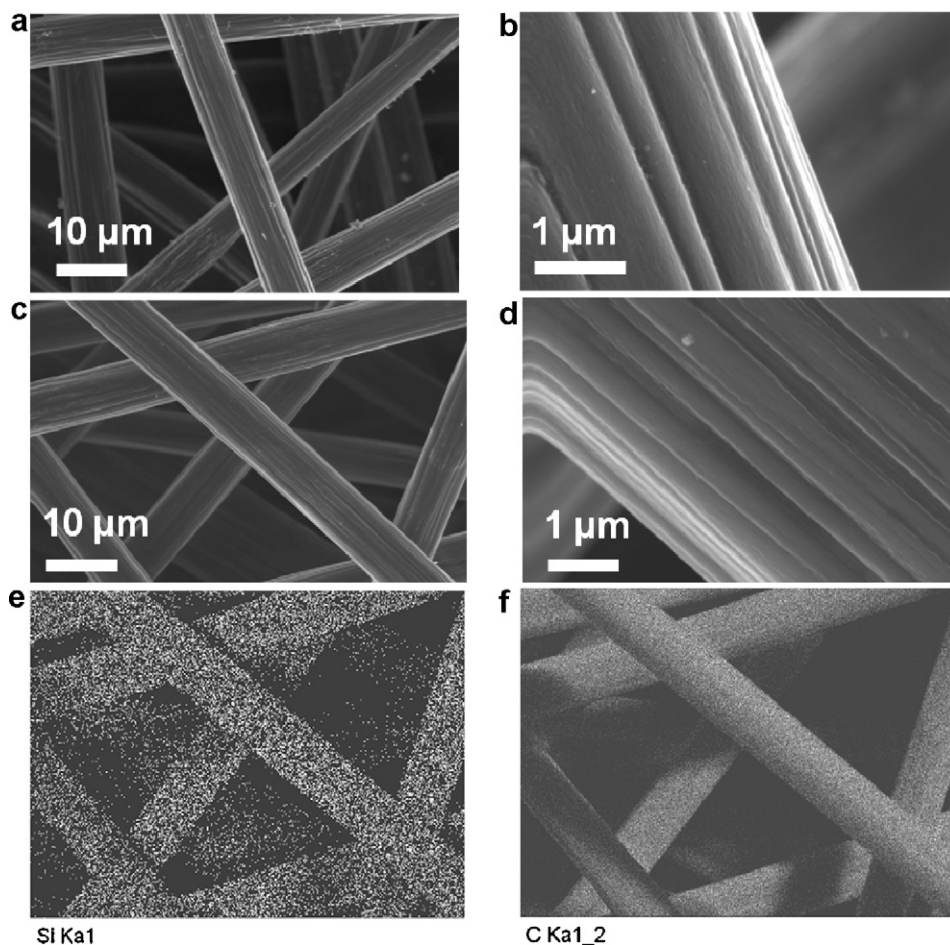


Figure 3 SEM images and corresponding EDX maps of the CP samples demonstrating their scaffold structure, smooth surface morphology and the homogeneity of the SiO₂ deposition on the carbon fibers. (a and b) SEM images of the CP. (c and d) SEM images of the SiO₂-CP. (e and f) Corresponding silicon and carbon EDX maps of the SiO₂-CP.

deposition/stripping cycling, which cannot be readily realized with coin or Swagelok cells. The cells were assembled in an argon-filled glove box. The CP electrode loadings were typically ~ 5.8 mg (0.5 cm²). Lithium metal foils were used as a counter/reference electrode. A 1.0M solution of LiPF₆ in a mixture of EC/EMC (3:7, v/v) was used as the electrolyte. The vial cell setup is schematically shown in Fig. 2. The working and counter electrodes were soaked in the electrolyte without any pressure applied on them. SiO₂-CP (SiC-CP) was attached onto a copper foil at the edges by dried Na₂SiO₃ solution. The copper foil has the same dimensions as the carbon paper electrode, to avoid an electrolyte exposure on the non-SiO₂ (or non-SiC) side. The copper surface opposite to the CP electrodes was shielded by spin coated and dried Na₂SiO₃ solution. The pristine CP electrode was assembled in the same manner.

Results and discussion

For a proof-of-concept study, we chose commercially available CP as the 3D current collector. We deposit SiO₂ onto one side of CP *via* an electron-beam evaporation method. Ideally, the insulating coating materials on the current collector exhibit superb chemical resistance, particularly in a

diluted HF solution. It has recently been discovered that a portion of fluorinated salts in electrolytes may thermally decompose and release HF into the electrolyte [49]. Motivated by this fact, the SiO₂ coating was later converted into SiC by a magnesiothermic reaction.

CP exhibits many desirable characteristics as a 3D current collector for lithium deposition, including limited surface area, large void volume, and good conductivity. According to N₂ sorption measurements, the CP that we used exhibits a Brunauer–Emmett–Teller (BET) specific surface area of 5.3 m² g⁻¹ and a Barrett–Joyner–Halenda (BJH) specific pore volume of 1.2 cm³ g⁻¹. It is well known that the parasite reactions between deposited lithium and aprotic solvents/salt anions are inevitable, and they result in a loss of metallic lithium mass in the formation of the SEI layer, typically several tens of nanometers thick [50]. Current collectors of a 3D structure with a relatively low surface area help limit the reactivity of the deposited lithium towards electrolytes. On the other hand, a large void volume is desirable to achieve a high deposition accommodation capacity. The well-resolved peaks in the wide angle X-ray diffraction (XRD) pattern (Fig. S1a) reveal a highly graphitic structure of the carbon fibers in CP. Measured by the four-point method, the graphitic CP exhibits a high conductivity of 31 S cm⁻¹ at room temperature, which is an order of magnitude higher

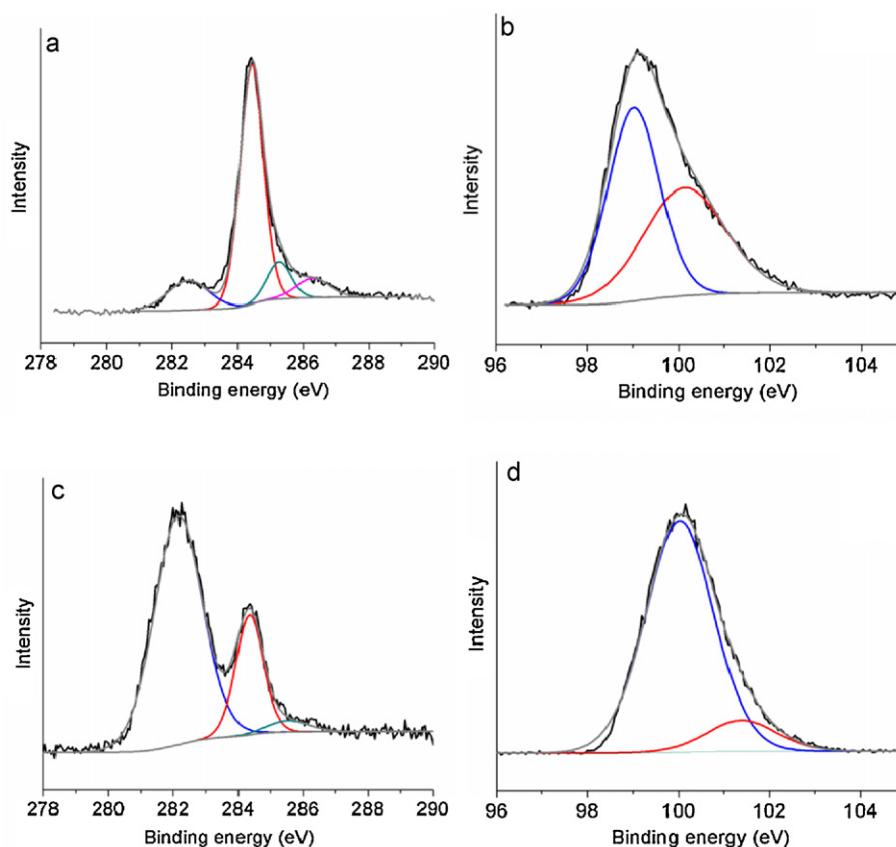


Figure 4 XPS spectra of the SiC decorated carbon paper samples, showing the SiC formation on the line-of-sight surface of carbon-fiber papers. (a) C [1s] of signal of SiC-CP-1 deconvoluted into components including a minor contribution from SiC (blue curve) at 282.5 eV. (b) Si [2p] signal of SiC-CP-1 deconvoluted into components including metallic silicon (blue curve) at 99.0 eV, and SiC (red curve) at 100.2 eV. (c) C [1s] of signal of SiC-CP-2 deconvoluted into components including a major contribution from SiC (blue curve) at 282.5 eV. (d) Si [2p] signal of SiC-CP-2 centered at 100.1 eV without any contribution from metallic silicon.

than its amorphous counterparts [17]. The CP is typically 200 (± 25) μm thick, slightly thicker than the commercial LIB anode layer ($\sim 150 \mu\text{m}$) composed of a copper foil current collector (18 μm) and a carbon electrode paste [51]. Scanning electron microscopy (SEM) images (Fig. 3a and Fig. S1b) reveal a scaffold-like morphology of CP which is constructed by carbon fibers that are 10–20 μm in diameter and contains interconnected voids sized from $\sim 50 \mu\text{m}$ to $\sim 100 \mu\text{m}$. The surface of carbon fibers appears fairly smooth at a 20,000 \times magnification (Fig. 3a and b). This provides a spacious volume for deposited lithium to grow into large crystals.

As a line-of-sight process [52], the SiO_2 e-beam evaporation coating is used here to selectively insulate the line-of-sight surface (also the electrolyte-facing surface) of the 3D current collector. The line-of-sight process is confirmed in our case by the fact that the silicon energy dispersive X-ray (EDX) map on the non- SiO_2 side of the carbon paper displayed very weak signals close to the background noise (see Fig. S2). After the SiO_2 deposition, the CP turns from dark-gray to a dark-brown color. The SEM image and the corresponding silicon EDX map reveal the homogeneity of the SiO_2 coating (Fig. 3c and e). It is evident that the surface of the carbon fibers stays smooth with a pinhole-free SiO_2 deposition (Fig. 3d). This implies impermeability to lithium ions from the electrolyte during lithium deposition.

We expected to form a SiC coating on the carbon fibers as well, in order to resist the potential HF etching in the electrolytes. It is challenging to form SiC coating on the

CP by conventional methods due to its high formation temperatures. Magnesiothermic reactions have been applied in converting a nanoporous silica film into a silicon film [53]. Recently, our group reported a low-temperature conversion reaction from a hierarchically ordered porous SiO_2 /carbon composite to a faithful SiC structure in the presence of hot magnesium vapor [54]. In the study here, we also used the magnesiothermic reaction to convert SiO_2 layer atop the carbon surface into SiC. We conducted X-ray photon spectra (XPS) measurements on the reacted CP. As Fig. 4a shows, the deconvoluted carbon [1s] signal exhibits the characteristic peak assigned to SiC at 282.5 eV. As revealed in Fig. 4b, the Si [2p] signal can be assigned to metallic silicon at 99.0 eV and SiC at 100.1 eV, respectively, and SiO_2 signal contribution is not observed. The atomic ratio between SiC and metallic Si is 47.2:52.8. The XPS results suggest that the carbon atomic diffusion did not permeate the SiO_2 /Si layer during the magnesiothermic reaction.

It is well known that silicon phase can be lithiated (alloyed with lithium) and potentially acts as plating sites during lithium deposition. Therefore, the SiC decorated CP samples were etched in an HF solution (50% weight) overnight. The CP sample after the magnesiothermic reaction and HF etching is referred to as SiC-CP-1. SEM images (Fig. 5a and b) reveal its rough surface morphology, in contrast to that of the pristine CP and SiO_2 -CP. The corresponding silicon EDX map remains intense and homogeneous on the surface of CP (Fig. 5c). Importantly, the roughness

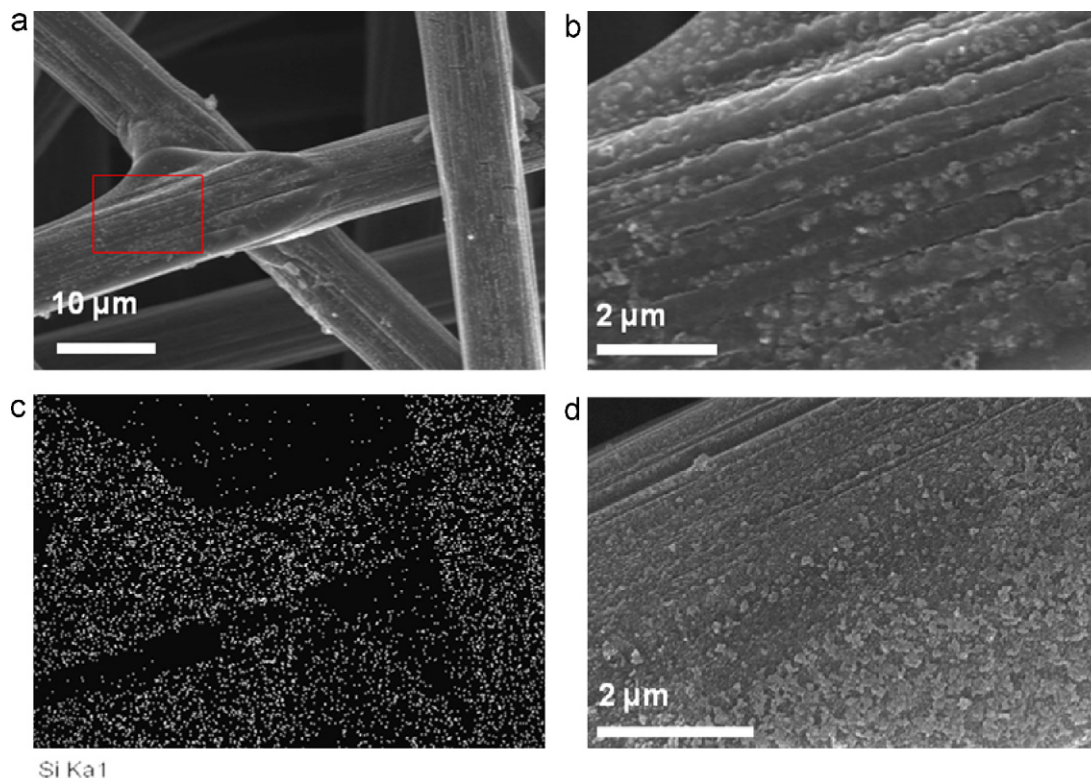


Figure 5 SEM images and corresponding EDX maps on SiC-CP samples. (a) A representative SEM image of SiC-CP-1. (b) Enlarged image of the inset red box in (a), revealing the rough surface morphology. (c) Silicon EDX mapping revealing the relatively homogenous presence of silicon on the line-of-sight surface of SiC-CP-1. (d) SEM image showing the surface morphology of SiC-CP-2.

is not continuous, indicating an incomplete coverage of SiC on the carbon fiber surface. In order to achieve the aimed spatial heterogeneity, the SiO₂ coating and magnesiothermic conversion were repeated once upon the SiC-CP-1. The obtained sample is referred to as SiC-CP-2. As shown in Fig. 5d, the line-of-sight surface of SiC-CP-2 is completely roughened, suggestive of a much better SiC coverage on the designated area of CP. XPS was used to characterize HF etched SiC-CP-2. As Fig. 4a and c shows, the minor C [1s] component at 282.5 assigned to the SiC phase from SiC-CP-1 turns into a major component in the C [1s] signal from SiC-CP-2, which confirms a better SiC coverage of SiC-CP-2 than Si-CP-1. As shown in Fig. 4d, SiC-CP-2 displays a Si [2p] signal centered at 100.1 eV that can be assigned to the SiC phase, without any contribution from metallic silicon.

We carried out lithium depositing on pristine CP, SiO₂-CP, SiC-CP-1 and SiC-CP-2 as working electrodes. For spatially heterogeneous CPs, only the insulated side was exposed to the electrolyte. In our study, we attempted to minimize the lithium intercalation reactions into the CP samples and focused on the lithium depositing behavior. Hence, a high

current density of $\sim 4 \text{ mA cm}^{-2}$ (330 mA g^{-1} carbon paper, based on 0.012 g cm^{-2} for CP) was applied between the working electrode and a lithium counter/reference electrode during the depositing process. This current density represents one of the highest values reported for lithium deposition studies, compared to current densities of less than 1 mA cm^{-2} in most previous studies [55]. The deposition process was carried out for 2 h, and the deposition capacity was set to be 28.8 C cm^{-2} (or 660 mAh g^{-1} carbon paper). To the best of our knowledge, this is the largest quantity of lithium deposition compared to previous dendrites related studies including those with protection layers. The deposition on SiO₂-CP was also done for 6 h to approach the limit of the accommodation capacity. As shown in Fig. S3, after several minutes of cathodic reactions on the working electrodes, the potentials of both CP and SiO₂-CP electrodes rapidly dropped below 0.0V vs. Li⁺/Li, indicating that metallic lithium deposition on the carbon fiber surface had started. Lithium intercalation into carbon is thermodynamically favorable; however, at potentials below 0.0V vs. Li⁺/Li, lithium plating on carbon surface is kinetically more facile. This leads to the fact that

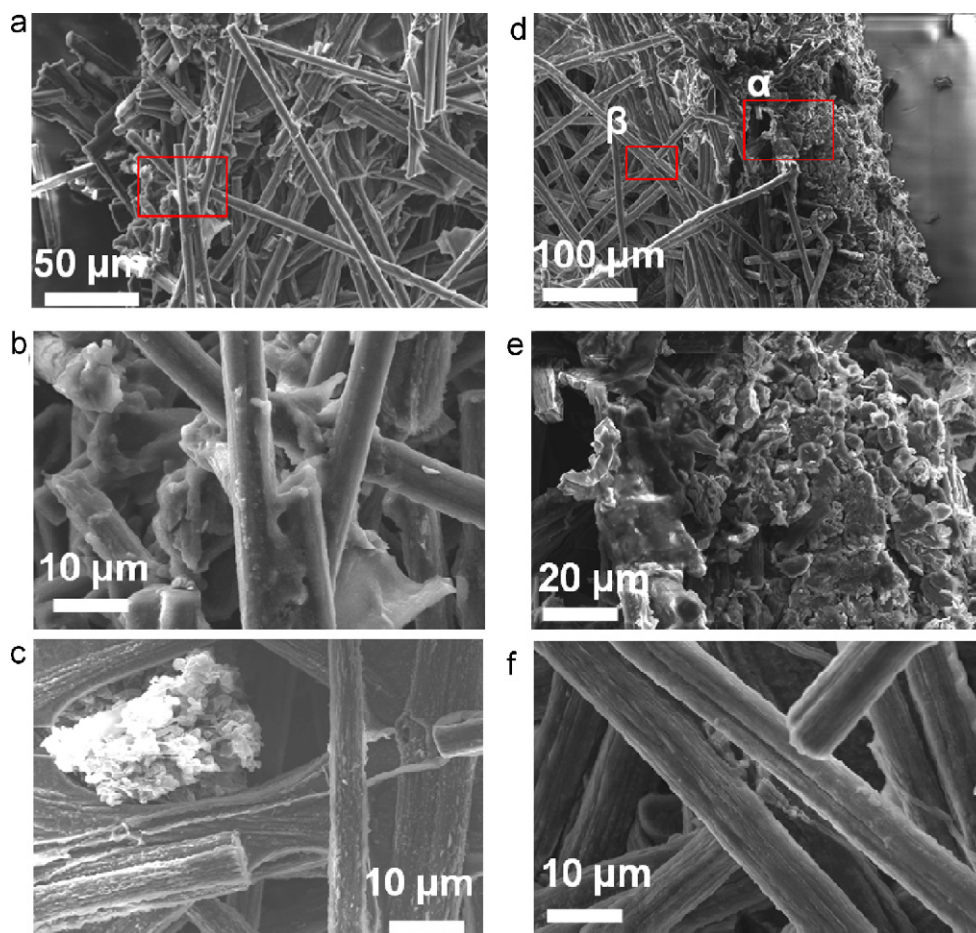


Figure 6 SEM images of cross-section areas of the lithium deposited CP and SiO₂-CP samples, showing the superior performances of the SiO₂-CP than the pristine CP in terms of dendrite control and lithium infiltration into the paper voids. (a) A representative SEM image of lithium deposited pristine CP. (b) Enlarged image of the inset in (a). (c) A representative SEM image showing the surface morphology of the lithium deposited CP and existence of formed dendrites. (d) A representative SEM image of the lithium deposited SiO₂-CP. (e) Enlarged image of inset α in (d). (f) Enlarged image of inset β in (d). All the images here were taken with the paper specimen stage tilted by 45°.

lithium-ion batteries on electric vehicles have to be charged for hours to prevent lithium plating [56].

The deposited electrodes were examined *ex situ* by SEM in order to investigate the “geographical” distribution of the deposited lithium metal. The SEM specimen stage was tilted by 45° in order to show both the cross-section and the adjacent face area of the lithium metal deposited CP electrodes. The cross-section of lithium metal deposited CP electrode displays a uniform morphology of carbon fibers (Fig. 6a and b). It is evident that lithium metal deposition did not infiltrate the voids of pristine CP. Fig. 6c reveals a representative area on the CP surface with large lithium metal dendrites over $20\ \mu\text{m}$ in size and small lithium metal crystals homogeneously distributed. The pristine CP electrode functions essentially as a two-dimensional current collector.

In sharp contrast, as shown by the SEM images (Fig. 6d–f), the voids near the bottom of the SiO_2 -CP were well infiltrated by lithium metal deposition. The deposited lithium metal crystals, closely packed, exhibit particle sizes in the range of 10 – $20\ \mu\text{m}$ (Fig. 6e). The surface morphology of the SiO_2 decorated area near the cross-section remains very smooth and free of deposited lithium crystallites or dendrites, as shown in Fig. 6f. This indicates that the SiO_2 coating is impermeable to lithium ions and has successfully created an insulating roof for the 3D current collector. A zoom-out view under SEM, confirms that the surface of deposited SiO_2 -CP is completely free of lithium dendrites and that the voids near the top surface are also free of lithium infiltration (Fig. S4). The lithium metal deposition into the SiO_2 -CP fills up the voids from the non-silica to the silica side, which is facilitated by the conducting copper foil support on the non- SiO_2 surface of the electrode and, more importantly, by the anisotropic structure of the current col-

lector. During lithium deposition, with no electrons available from the SiO_2 surface, lithium ions driven by the electric field migrated deeper into the voids inside the porous current collector where they were reduced. As Fig. S5 shows, lithium deposition occurs on the conducting carbon surface which is oppositely oriented towards the SiO_2 coated electrode surface. After lithium deposition for 6 h, the SiO_2 -CP was nearly fully infiltrated by deposited lithium, as revealed by the solid edge part of the paper under the *ex situ* SEM investigation (Fig. S6). The deposited lithium provided a capacity of $86.4\ \text{C cm}^{-2}$ (or $1980\ \text{mA h g}^{-1}$ carbon paper), which is tantalizingly near (81%) $106.9\ \text{C cm}^{-2}$ ($2474\ \text{mA h g}^{-1}$ carbon paper), the theoretical accommodation capacity calculated based on the specific pore volume of $1.2\ \text{cm}^3\ \text{g}^{-1}$ and lithium metal density. It is worth noting that further deposition on a fully infiltrated 3D current collector may result in the dendrite growth on the filled paper top surface. Therefore, it is important to prevent an over-infiltration during the deposition cycle in practical scenarios. The spatially controlled lithium deposition resembles in some degree the single-crystal growth of calcium carbonate in the assembly process that generates the abalone cell [57]. Compared to the deposition on pristine CP, the surface SiO_2 coating effectively realizes the proposed function of a spatially heterogeneous structure.

The cross-section of the lithium deposited SiC-CP-1 is shown in Fig. 7a. It is evident that lithium infiltration took place in the voids, as shown in Fig. 7b. However, some plated lithium phase can be observed on the SiC decorated surface (Fig. 7c), which we found was due to the discontinuity of the nano-crystalline SiC coating on the SiC-CP-1. On the SiC-CP-2, with a complete SiC coverage, it is confirmed that the SiC double coated area is dendrite-free, as shown in Fig. 7d.

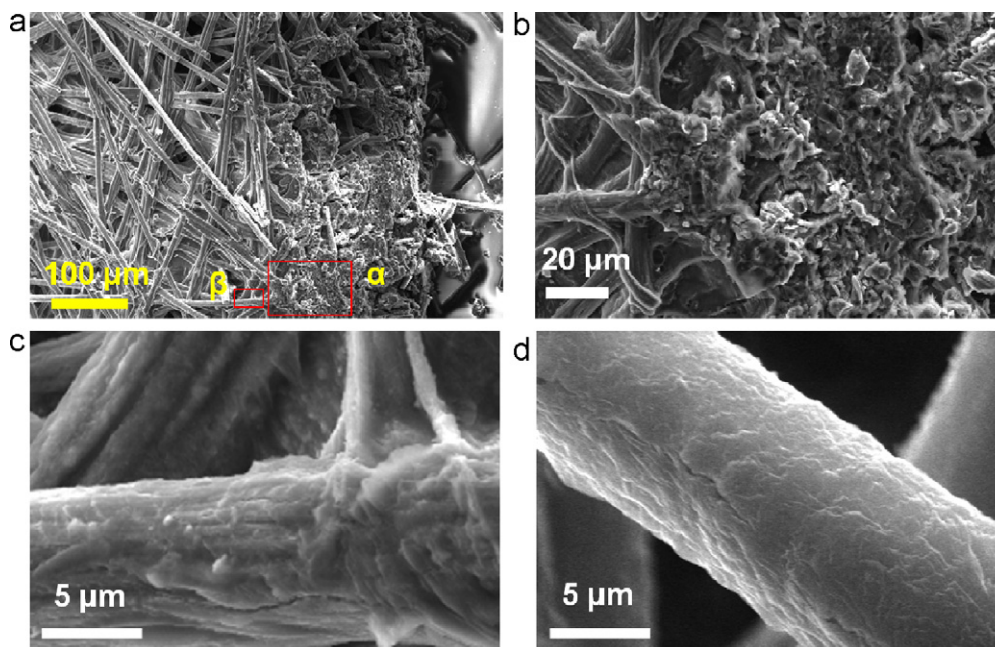


Figure 7 SEM images of the cross-section area of the lithium plated SiC-CP samples. (a) An overview image of the cross-section area of SiC-CP-1. (b) Enlarged image of inset α in (a). (c) Enlarged image of inset β in (a). (d) A representative SEM image of carbon fibers in the line-of-sight surface of lithium deposited SiC-CP-2. All the images were taken with the paper specimen stage tilted by 45° .

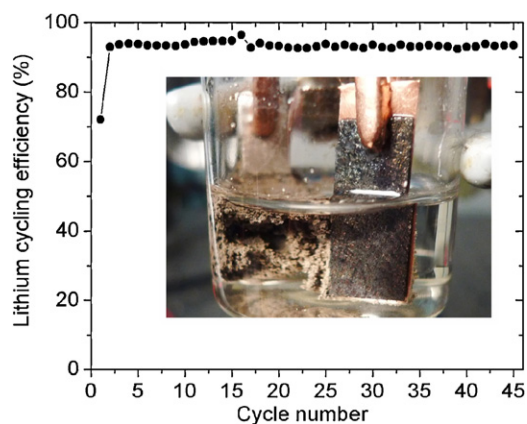


Figure 8 Coulombic efficiency for the lithium depositing/stripping cycling process on the SiC-CP-2 current collector, revealing the superior disposition performance, inset: an image of the vial cell containing SiC-CP-2 working electrode and lithium foil counter electrode, taken after 15 cycles, showing the dendrite-free surface of SiC-CP-2 current collector and mossy lithium phase formed around the lithium counter electrode.

This indicates that a HF resisting spatial heterogeneity has been created in the SiC-CP-2.

Repeated deposition/stripping on SiC-CP-2 were conducted to investigate the reversibility of the dendrite-free deposition. The deposition and stripping current density was set to be 2 mA cm^{-2} (or 165 mA g^{-1} carbon paper), and lithium of 14.4 C cm^{-2} (or 330 mA g^{-1} carbon paper) was deposited. The cut-off potential was set to be 3.0 V versus Li^+/Li for lithium

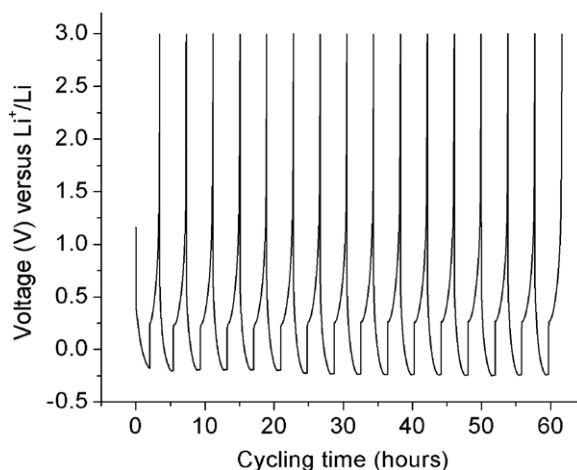


Figure 9 Lithium depositing/stripping profiles on SiC-CP-2 (the first 15 cycles), plotted on voltage versus time, at a current density of 2 mA cm^{-2} and a lithium deposition of 14.4 C cm^{-2} (330 mA h g^{-1} carbon paper).

stripping. By deep deposition/stripping processes, we put the 3D current collectors in a more dendrite favored scenario to test the efficacy of the spatial heterogeneity concept. Fig. 8 shows the lithium cycling efficiency on the SiC-CP-2 current collector. Note that the low coulombic efficiency in the first cycle is due to SEI formation on the carbon surface, which is widely observed for carbon electrodes in the first discharge/charge cycle [58].

SiC-CP-2 displays a very stable lithium stripping/deposition efficiency of $\sim 94\%$ starting with the

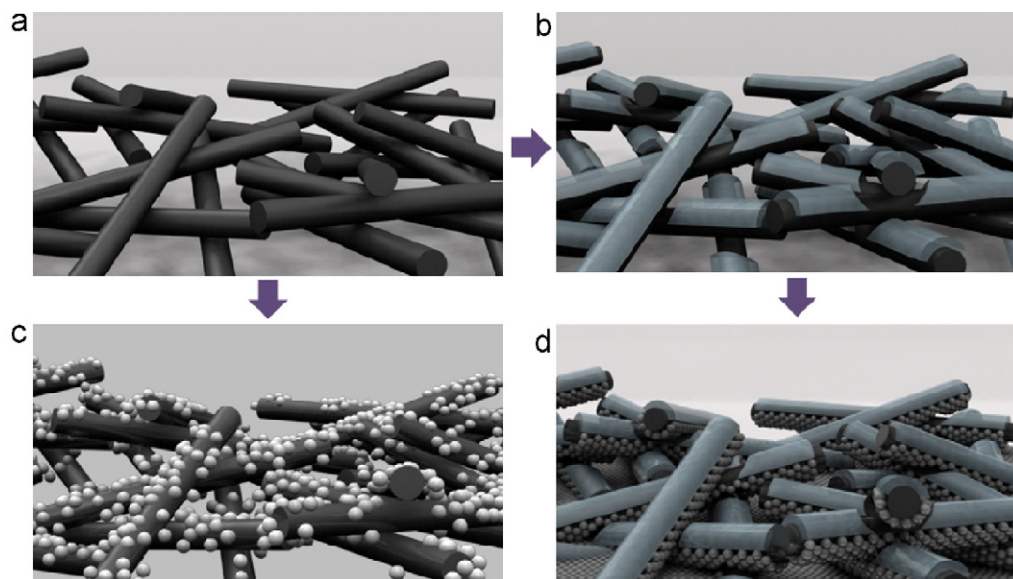


Figure 10 Schematic illustrating the structures of pristine CP and spatially heterogeneous CP (SH-CP), and the different lithium deposition processes on them. (a) CP. (b) SH-CP. Anisotropic spatial heterogeneity is achieved after a line-of-sight deposition of SiO_2 onto the carbon fibers. Light blue areas represent a SiO_2 or SiC coating, and black areas represent uncovered conducting carbon surface. (c) The situation of lithium deposition on CP, mostly on the line-of-sight surface. (d) The situation of lithium deposition in SH-CP. Lithium electrodeposition does not take place on the insulating line-of-sight surface but is driven by the electric field towards voids of the current collector. The silver spheres represent lithium atoms in (c) and (d).

second cycle. This is one of the highest lithium-cycling efficiencies reported for aprotic organic electrolytes [59–61]. It is worth stressing that the high efficiency is achieved at a current rate of 2 mA cm^{-2} and a deep lithium deposition of 14.4 C cm^{-2} in a carbonate based organic electrolyte, in contrast to previously reported lower efficiencies of around 70–90% typically obtained by using current rates less than 1 mA cm^{-2} , a lithium deposition less than 2 C cm^{-2} , and certain surface protection methods in favorable organic electrolytes [59,60,62]. Note that the internal surface area of a 3D current collector is much larger than its footprint area, which is a significant advantage than 2D ones. This could be an important factor that leads to the high coulombic efficiency.

It is well known that the lithium cycling efficiency is strongly influenced by the morphology of the deposited lithium [60]. The high cycling efficiency obtained here corroborates the ex situ SEM observation that deposited lithium is closely packed in the voids of the 3D current collectors. This clearly illustrates the superiority of the lithium deposition into 3D current collectors facilitated by a spatially heterogeneous structure. As shown by the inset of Fig. 8, at the end of the 15th cycle, the lithium counter electrode was covered by isolated mossy lithium accumulated over the deep deposition/stripping cycling; however, in sharp contrast, the SiC-CP-2 current collector retained a dendrite-free surface. Fig. 9 shows the deposition/stripping cycling profiles for the first 15 cycles. It is evident that at the current rate of 2 mA cm^{-2} , lithium deposition on SiC-CP-2 mainly takes place at potentials below 0 V versus Li^+/Li , which indicates that lithium plating on the carbon surface, instead of Li-ion intercalation into carbon structure, is the major process. Nevertheless, it is reasonable to believe that the intercalation effect might have a minor contribution to the high lithium cycling efficiency.

We are aware that a lithium cycling efficiency of up to 99.2% can be achieved with ionic liquid based [29] or polymer based [26] electrolytes. However, these high efficiencies were obtained at lower current densities and lower lithium deposition rates than the conditions in this report. Despite the high efficiencies achieved in these superior electrolytes, even at the lower current densities and lithium deposition rates that were used, the morphology of the deposited lithium is still highly mossy [27]. It is our purpose in this report to use a more common organic electrolyte to demonstrate the advantages of spatially heterogeneous 3D current collectors for both lithium cycling efficiency and dendrite control. Meanwhile, research on combining ionic liquid electrolytes and 3D current collectors is ongoing in our laboratory.

Conclusions

As schematically shown in Fig. 10b, spatially heterogeneous insulating/conducting properties of the CP can be obtained after the SiO_2 electron-beam deposition. The same spatial heterogeneity can be maintained by converting SiO_2 into SiC atop the carbon paper surface. This anisotropic spatial heterogeneity is essential in order to achieve surface dendrite-free lithium deposition on the SiO_2 -CP or SiC-CP current collectors, as schematically shown in Fig. 10d. With

the large porous volume of the current collector effectively utilized by lithium deposition, the electrode maintains a constant volume upon deposition. Moreover, due to the scaffold-like structure of the carbon paper, disintegration of deposited lithium [63] cannot occur inside the paper in the presence of nearby 3D electric contacts at a high depositing rate. The stable lithium cycling efficiency of 94% achieved in SiC-CP-2 in a carbonate based organic electrolyte further demonstrates the superiority of the anisotropic spatial heterogeneity of the 3D current collector.

Our approach on addressing the dendrite formation problem represents a fundamentally new concept *via* rationally designed current collectors with heterogeneous properties. Other 3D architectures such as carbon cloth, carbon nanotube infiltrated papers and those made with copper, aluminum or conducting ceramics should show similar performances. Other systems with metallic electrodes, e.g. magnesium batteries may be benefited from this method as well. Please note that there are still hurdles to cross before a lithium metal anode is completely ready for commercial applications. Extensive further efforts are being made in order to reach this goal.

Acknowledgements

The work was supported by the National Science Foundation No. DMR 0805148, University of California Lab Fees Program (09-LR-08-116809-STUG), and a postdoctoral fellowship from the Natural Sciences and Engineering Research Council of Canada (awarded to X. Ji). This work made use of MRL Central Facilities supported by the MRSEC Program of the National Science Foundation (DMR05-20415) and UCSB Nanofabrication Facility. We thank Dr. Jeffrey Gerbec for his assistance with the electrochemical instruments. We thank Professor Martin Moskovits and Dr. Syed Mubeen Jawahar Hussaini for helpful discussions.

Appendix A. Supplementary data

Supplementary data associated with this article can be found, in the online version, at doi:10.1016/j.nantod.2011.11.002.

References

- [1] T. Nagaura, K. Tozawa, Prog. Batteries Solar Cells 9 (1990) 209–217.
- [2] J.S. Dunning, W.H. Tiedemann, L. Hsueh, D.N. Bennion, J. Electrochem. Soc. 118 (1971) 1886–1890.
- [3] M.S. Whittingham, US Patent 4,009,052 (1977).
- [4] G.-A. Nazri, G. Pistoia (Eds.), Lithium Batteries Science and Technology, Kluwer Academic Publishers, 2004.
- [5] I. Epelboin, M. Froment, M. Garreau, J. Thevenin, D. Warin, Proc. Electrochem. Soc. 80 (4) (1980) 417–429.
- [6] R. Bhattacharyya, B. Key, H. Chen, A.S. Best, A.F. Hollenkamp, C.P. Grey, Nat. Mater. 9 (2010) 504–510.
- [7] Y. Cohen, D. Aurbach, J. Phys. Chem. B 104 (2000) 12282–12291.
- [8] D. Aurbach, Y. Cohen, J. Electrochem. Soc. 143 (1996) 3525–3532.
- [9] A. Teyssot, C. Belhomme, R. Bouchet, M. Rosso, S. Lascaud, M. Armand, J. Electroanal. Chem. 584 (2005) 70–74.

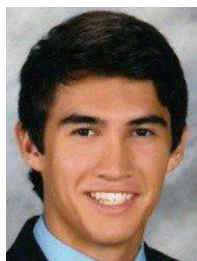
- [10] D.W. Murphy, F.J. DiSalvo, J.N. Carides, J.V. Waszczak, *Mater. Res. Bull.* 13 (1978) 1395–1402.
- [11] M. Lazzari, B. Scrosati, *J. Electrochem. Soc.* 127 (1980) 773–774.
- [12] J.B. Goodenough, Y. Kim, *Chem. Mater.* 22 (2010) 587–603.
- [13] B.L. Ellis, K.T. Lee, L.F. Nazar, *Chem. Mater.* 22 (2010) 691–714.
- [14] Y.J. Lee, H. Yi, W.-J. Kim, K. Kang, D.S. Yun, M.S. Strano, G. Ceder, A.M. Belcher, *Science* 324 (2009) 1051–1055.
- [15] H.L. Zhang, D.E. Morse, *J. Mater. Chem.* 19 (2009) 9006–9011.
- [16] B. Scrosati, J. Garche, *J. Power Sources* 195 (2010) 2419–2430.
- [17] X. Ji, K.T. Lee, L.F. Nazar, *Nat. Mater.* 8 (2009) 500–506.
- [18] K.M. Abraham, Z. Jiang, *J. Electrochem. Soc.* 143 (1996) 1–5.
- [19] E. Yoo, H. Zhou, *ACS Nano* 5 (2011) 3020–3026.
- [20] X. Ji, S. Evers, R. Black, L.F. Nazar, *Nat. Commun.* (2011), doi:10.1038/ncomms1293.
- [21] G. He, X. Ji, L.F. Nazar, *Energy Environ. Sci.* 4 (2011) 2878–2883.
- [22] J.-S. Lee, S.T. Kim, R. Cao, N.-S. Choi, M. Liu, K.T. Lee, J. Cho, *Adv. Energy Mater.* 1 (2011) 34–50.
- [23] J.-N. Chazalviel, *Phys. Rev. A* 42 (1990) 7355–7367.
- [24] M. Rosso, T. Gobron, C. Brissot, J.-N. Chazalviel, S. Lascaud, *J. Power Sources* 97–98 (2001) 804–806.
- [25] M. Armand, W. Gorecki, R. Andréani, B. Scrosati (Eds.), *Second Int. Symp. on Polymer Electrolytes*, Elsevier, London, 1990, p. 91.
- [26] L. Sannier, R. Bouchet, L. Santinacci, S. Grugeon, J.-M. Tarascon, *J. Electrochem. Soc.* 151 (2004) A873–A879.
- [27] L. Sannier, R. Bouchet, M. Rosso, J.-M. Tarascon, *J. Power Sources* 158 (2006) 564–570.
- [28] N. Byrne, P.C. Howlett, D.R. MacFarlane, M. Forsyth, *Adv. Mater.* 17 (2005) 2497–2501.
- [29] G.T. Kim, G.B. Appetecchi, M. Montanino, F. Alessandrini, S. Passerini, *ECS Trans.* 25 (2010) 127–138.
- [30] H. Ota, Y. Sakata, Y. Otake, K. Shima, M. Ue, J. Yamaki, *J. Electrochem. Soc.* 15 (2004) A1778–A1788.
- [31] K. Kanamura, S. Shiraishi, Z. Takehara, *J. Electrochem. Soc.* 141 (1994) L108–L110.
- [32] F. Marchioni, K. Star, E. Menke, T. Buffeteau, L. Servant, B. Dunn, F. Wudl, *Langmuir* 23 (2007) 11597–11602.
- [33] G.A. Umeda, E. Menke, M. Richard, K.L. Stamm, F. Wudl, B. Dunn, *J. Mater. Chem.* 21 (2011) 1593–1599.
- [34] C. Liebenow, K. Lühder, *J. Appl. Electrochem.* 26 (1996) 689–692.
- [35] Y.M. Lee, N.-S. Choi, J.H. Park, J.-K. Park, *J. Power Sources* 119–121 (2003) 964–972.
- [36] J.B. Bates, N.J. Dudney, G.R. Gruzalski, R.A. Zuhr, A. Choudhury, C.F. Luck, *J. Power Sources* 43–44 (1993) 103–110.
- [37] S.J. Visco, F.Y. Tsang, *US Patent* 6,214,061 (2001).
- [38] S.J. Visco, E. Nomon, B. Katz, L.C.D. Jogle, M.Y. Chu, *The 12th International Meeting on Lithium Batteries*, Nara, Japan, Abstract #53, 2004.
- [39] S.J. Visco, Y.S. Nimon, B.D. Katz, *US Patent* 7,390,591 (2008).
- [40] T.A. Skotheim, C.J. Sheehan, Y.V. Mikhaylik, J. Affinito, *US Patent* 6,936,381 (2005).
- [41] S.J. Visco, Y.S. Nimon, B.D. Katz, *US Patent* 7,282,302 (2007).
- [42] J. Elezgaray, C. Léger, F. Argoul, *Phys. Rev. Lett.* 84 (2000) 3129–3132.
- [43] K. Okita, K. Ikeda, H. Sano, Y. Iriyama, H. Sakaebe, *J. Power Sources* 196 (2011) 2135–2142.
- [44] Y.J. Lee, Y. Lee, D. Oh, T. Chen, G. Ceder, A.M. Belcher, *Nano Lett.* 10 (2010) 2433–2440.
- [45] P.L. Taberna, S. Mitra, P. Poizot, P. Simon, J.-M. Tarascon, *Nat. Mater.* 5 (2006) 567–573.
- [46] M.S. Yazici, D. Krassowski, J. Prakash, *J. Power Sources* 141 (2005) 171–176.
- [47] C. Arbizzani, M. Lazzari, M. Mastragostino, *J. Electrochem. Soc.* 152 (2010) A289–A294.
- [48] L.H.S. Gasparotto, A. Prowald, N. Borisenko, S. Zein El Abedin, A. Garsuch, F. Endres, *J. Power Sources* 196 (2011) 2879–2883.
- [49] B. Markovsky, F. Amalraj, H.E. Gottlieb, Y. Gofer, S.K. Martha, D. Aurbach, *J. Electrochem. Soc.* 157 (2010) A423–A429.
- [50] D. Aurbach, I. Weissman, A. Schechter, *Langmuir* 12 (1996) 3991–4007.
- [51] R. Moshkev, B. Johnson, *J. Power Sources* 91 (2000) 86–91.
- [52] D.M. Mattox, *Vacuum deposition, reactive evaporation and gas evaporation*, in: *ASM Handbook*, ASM Publ. 5, Surface Engineering, 1994, pp. 556–572.
- [53] E.K. Richman, C.B. Kang, T. Brezesinski, S.H. Tolbert, *Nano Lett.* 8 (2008) 3075–3079.
- [54] Y. Shi, F. Zhang, Y.-S. Hu, X. Sun, Y. Zhang, H.I. Lee, L. Chen, G.D. Stucky, *J. Am. Chem. Soc.* 132 (2010) 5552–5553.
- [55] H. Honbo, K. Takei, Y. Ishii, T. Nishida, *J. Power Sources* 189 (2009) 337–343.
- [56] K. Eberman, P.M. Gomadam, G. Jain, E. Scott, *ECS Trans.* 25 (2010) 47–58.
- [57] C.M. Zaremba, A.M. Belcher, M. Fritz, Y. Li, S. Mann, P.K. Hansma, D.E. Morse, J.S. Speck, G.D. Stucky, *Chem. Mater.* 8 (1996) 679–690.
- [58] M. Winter, J.O. Besenhard, M.E. Spahr, P.E. Novák, *Adv. Mater.* 10 (1998) 725–763.
- [59] H. Ota, Y. Sakata, Y. Otake, K. Shima, M. Ue, J. Yamaki, *J. Electrochem. Soc.* 151 (2004) A1778–A1788.
- [60] H. Ota, X. Wang, E. Yasukawa, *J. Electrochem. Soc.* 151 (2004) A427–A436.
- [61] D. Aurbach, A. Zaban, A. Schechter, Y. Ein-Eli, E. Zinigrad, B. Markovsky, *J. Electrochem. Soc.* 142 (1995) 2873–2882.
- [62] S. Shiraishi, K. Kanamura, Z. Takehara, *J. Electrochem. Soc.* 146 (1999) 1633–1639.
- [63] D. Aurbach, E. Zinigrad, H. Teller, P. Dan, *J. Electrochem. Soc.* 147 (2000) 1274–1279.



Xiulei (David) Ji received his B.Sc. in Chemistry from Jilin University in 2003. He obtained his Ph.D. in Materials Chemistry from the University of Waterloo in 2009, under the supervision of Professor Linda F. Nazar. At Waterloo, he worked on Li–S batteries and fuel cell catalysts. In Professor Galen D. Stucky’s group, he has been working on new energy devices and rationally designed materials and structures for energy purposes. He was awarded a Postdoctoral Fellowship from Natural Sciences and Engineering Research Canada (NSERC), the NSERC Innovation Challenge Award 2010, and Chinese Government Award for Outstanding Students Studying Abroad 2008.



De-Yu Liu received his B.Sc. in Chemistry at Xiamen University in 2009, China. His work mainly focused on the synthesis and optical properties of surface plasmonic nanostructures. At UCSB he has been working on photocatalysis and energy efficient materials. De-Yu Liu has co-authored 4 peer reviewed papers.



Daniel Prendiville is currently working towards his B.Sc. in Biological Sciences at University of California Santa Barbara. He has served as an undergraduate research assistant on various projects focusing on biosystem processes and energy challenges.



Yichi Zhang received his B.Sc. in Chemistry at Peking University, Beijing, China. At UCSB, he is mainly working on the energy related materials such as high efficient thermoelectrics for his Ph.D. study in Chemical Materials. Now he is a Ph.D. candidate with 8 first-authored and co-authored peer reviewed papers in the top journals such as J. Am. Chem. Soc., Adv. Mater., ACS Nano, etc.



Xiaonao Liu received her B.Eng. in Printing Engineering (2003) and her Ph.D. in pulp and paper making engineering from Tianjin University of Science and Technology (2008). In August 2008, she joined the Fan group (Zhejiang University, China) as a postdoctoral fellow. She is currently an associate research fellow of Chemistry at Zhejiang University. Her research centers on combinatorial synthesis and optimization mesostructure materials for energy and environment.

ronment.



Galen D. Stucky received his Ph.D. in 1962 from Iowa State University. After a postdoctoral study at MIT, he held positions at the University of Illinois, Sandia National Laboratory and DuPont Central Research and Development Department before joining the UCSB faculty in 1985. Recent honors include the ACS Award in Chemistry of Materials (2002), the International Mesostructured Materials Association Award (2004), and election to fellowship in the American Academy of Arts and Sciences (2005). He is currently the E. Khashoggi Industries, LLC Professor in Letters and Science at UCSB.